Turbulent mixing in a strongly forced salt wedge estuary

David K. Ralston,[1] W. Rockwell Geyer,[1] James A. Lerczak,[2] and Malcolm Scully[3]

Received 18 December 2009; revised 9 August 2010; accepted 8 September 2010; published 9 December 2010.

[1] Turbulent mixing of salt is examined in a shallow salt wedge estuary with strong fluvial and tidal forcing. A numerical model of the Merrimack River estuary is used to quantify turbulent stress, shear production, and buoyancy flux. Little mixing occurs during flood tides despite strong velocities because bottom boundary layer turbulence is dislocated from stratification elevated in the water column. During ebbs, bottom salinity fronts form at a series of bathymetric transitions. At the fronts, near-bottom velocity and shear stress are low, but shear, stress, and buoyancy flux are elevated at the pycnocline. Internal shear layers provide the dominant source of mixing during the early ebb. Later in the ebb, the pycnocline broadens and moves down such that boundary layer turbulence dominates mixing. Mixing occurs primarily during ebbs, with internal shear mixing accounting for about 50% of the total buoyancy flux. Both the relative contribution of internal shear mixing and the mixing efficiency increase with discharge, with bulk mixing efficiencies between 0.02 and 0.07. Buoyancy fluxes in the estuary increase with discharge up to about 400 m^3 s^{-1} above which a majority of the mixing occurs offshore. Observed buoyancy fluxes were more consistent with the k-ε turbulence closure than the Mellor-Yamada closure, and more total mixing occurred in the estuary with k-ε. Calculated buoyancy fluxes were sensitive to horizontal grid resolution, as a lower resolution grid yielded less integrated buoyancy flux in the estuary and exported lower salinity water but likely had greater numerical mixing.

Citation: Ralston, D. K., W. R. Geyer, J. A. Lerczak, and M. Scully (2010), Turbulent mixing in a strongly forced salt wedge estuary, *J. Geophys. Res.*, *115*, C12024, doi:10.1029/2009JC006061.

1. Introduction

[2] Turbulent mixing of salt and freshwater in estuaries affects the stratification, the length of the salinity intrusion, and the exchange of biological or chemical constituents between the river and coastal ocean. Where, when, and how that mixing occurs depends on the estuarine forcing. Previous work has examined turbulence and mixing in partially stratified estuaries like the Hudson River [*Peters*, 1999; *Trowbridge et al.*, 1999; *Chant et al.*, 2007] and San Francisco Bay [*Stacey et al.*, 1999]. Observations in partially mixed estuaries have found that bottom boundary layer shear is the dominant source of turbulence [*Trowbridge et al.*, 1999] and that salinity mixing occurs primarily due to bottom boundary layer turbulence during flood tides [*Peters*, 1999; *MacCready and Geyer*, 2001; *Chant et al.*, 2007]. Turbulence is generated at the bed and decreases in energy with distance above the bed due to overlying stratification, particularly during ebbs when tidal straining helps to maintain stratification [*Stacey et al.*, 1999].

[3] In contrast, observations in strongly stratified estuaries have noted the importance of interfacial shear instabilities for mixing [*Partch and Smith*, 1978; *Geyer and Farmer*, 1989; *Uncles and Stephens*, 1996; *Jay and Smith*, 1990a; *Kay and Jay*, 2003; *MacDonald and Horner-Devine*, 2008]. Strong shear can develop across the pycnocline during ebbs in tidal salt wedge estuaries leading to turbulence and mixing that is maximal midwater column, while bottom boundary layer mixing is relatively weak. The differences between partially and highly stratified estuaries indicate that the magnitude, mechanisms, and phasing of vertical salt flux vary through estuarine parameter space. How these mixing processes depend on estuarine characteristics like river discharge, tidal amplitude, and bathymetry remains to be quantified.

[4] The focus here is on turbulent salt flux in an estuary where river and tidal velocities are significant and steady baroclinic circulation is comparatively weak. The study site is the Merrimack River on the northeast coast of the United States, but conditions in the Merrimack are representative of time-dependent salt wedge estuaries like the Columbia [*Jay and Smith*, 1990b], Connecticut [*Garvine*, 1975], Fraser [*Geyer and Farmer*, 1989], and Snohomish River [*Wang et al.*, 2009] estuaries. These estuaries are short (the length of the salinity intrusion is similar to the tidal excursion),

[1]Applied Ocean Physics and Engineering, Woods Hole Oceanographic Institution, Woods Hole, Massachusetts, USA.
[2]College of Oceanic and Atmospheric Sciences, Oregon State University, Corvallis, Oregon, USA.
[3]Department of Ocean, Earth, and Atmospheric Sciences, Old Dominion University, Norfolk, Virginia, USA.

0148-0227/10/2009JC006061

strongly stratified, and have strong along-estuary salinity gradients. Recent work in the Merrimack has described the structure and variability of the salinity and velocity fields and longitudinal salt flux mechanisms [*Ralston et al.*, 2010].

[5] The goal here is to characterize and quantify turbulent mixing in a tidal salt wedge estuary, including how much mixing occurs, when mixing happens during the tidal cycle, where mixing occurs in the estuary, and what turbulence generation mechanisms are responsible. Turbulence and mixing are notoriously difficult to quantify in the field, so our approach is to use a numerical model that has been validated against extensive observations of salinity and velocity. Turbulence and mixing are calculated in the model and are evaluated over a range of forcing conditions, including seasonal variability in river discharge and spring-neap variability in tidal amplitude. Mixing mechanisms are expected to vary with forcing and to affect the location and efficiency of turbulent salt flux. We evaluate the model results by comparison with observations of turbulence in the Merrimack and consider the sensitivity of the results to turbulence closure and grid resolution.

2. Methods

2.1. Site Description

[6] The Merrimack River flows into the Gulf of Maine with a mean annual discharge of 220 $m^3 s^{-1}$. Seasonally, the discharge ranges from about 1500 $m^3 s^{-1}$ during the spring freshet to less than 50 $m^3 s^{-1}$ in late summer. The lower 35 km of the river are tidal, with a mean tidal range at the mouth of 2.5 m and a spring tidal range of about 4 m. In the upper estuary, the channel is narrow with a series of sills (typical depth of 4–6 m) and deeper holes (typical depth of 8–10 m) (Figure 1). Between 1.5 and 5 km from the mouth the estuary broadens into an embayment with intertidal flats and fringing salt marsh. The channel at the mouth passes between barrier islands and is constrained by rock jetties. A shallow ebb tide bar (4 m deep) is located about 0.5 km offshore of the mouth.

2.2. Observations

[7] Observations from moored instruments and shipboard surveys in the Merrimack during the spring and summer of 2005 were used to develop and calibrate the numerical model [*Ralston et al.*, 2010] Along-channel and across-channel mooring arrays measured surface elevation, velocity profiles, and surface and bottom salinities. Tidal cycle surveys were conducted to record the along-channel salinity distribution and the lateral salinity and velocity distributions at cross sections in the estuary. Hydrographic surveys corresponded with river discharges of 250, 550, and 350 $m^3 s^{-1}$.

[8] Additional observations were made in May 2007 using the Measurement Array for Sensing Turbulence (MAST) [*Geyer et al.*, 2008]. The MAST is a 10 m long spar with instrument brackets at multiple elevations to measure turbulent fluctuations in velocity and salinity. Each bracket holds an acoustic Doppler velocimter (ADV, sampling at 25 Hz) and a fast response conductivity sensor (sampling at 200 Hz) with sampling volumes offset by 2 cm in the flow direction. Salinity dominates the conductivity signal, so the colocated measurements at turbulent time scales allow direct covariance estimates of vertical salt flux $\overline{s'w'}$. Additional instruments on the MAST include conductivity-temperature (CT) and pressure sensors. The MAST is attached to a research vessel and provides continuous time series of turbulent mixing at multiple elevations spanning most of the estuarine water column.

[9] The MAST was used in the Merrimack in May 2007 over 3 days with moderate river discharge (350 $m^3 s^{-1}$) and tidal amplitude (2.6 m range). The MAST was deployed from an anchored research vessel in 6–8 m water depth (location shown in Figure 1). A second research vessel conducted simultaneous along- and across-channel surveys of salinity and velocity in the vicinity of the anchor site. Details on the MAST data processing can be found in the work of *Geyer et al.* [2008].

2.3. Numerical Model

[10] We have developed a numerical model of the Merrimack using the Finite Volume Coastal Ocean Model [*Chen et al.*, 2003, 2008]. FVCOM uses an unstructured horizontal grid of triangles and sigma layers vertically (Figure 1), and the finite volume approach is locally and globally conservative for momentum and scalars. The advection scheme is second-order accurate, and in test domains the accuracy compared well with higher-order advection schemes in a structured grid model [*Huang et al.*, 2008]. Horizontal grid resolution varied from about 20 m in the estuarine channel to about 3000 m near the offshore boundary; note that the offshore open boundaries are approximately 35 km from the river mouth (not shown in Figure 1). FVCOM includes wetting and drying, with cells becoming inactive when water level is less than 0.05 m. Twenty sigma levels were used vertically. Ten vertical levels provided insufficient resolution of the vertical structure of salinity and velocity, but simulations with 30 levels were quantitatively similar to 20 level cases. Note that temperature is not modeled because salinity dominates the density variations.

[11] The bathymetry for the model grid was based on NOAA soundings and was refined with additional bathymetric data collected in 2005 and 2007. Boundary conditions included tidal forcing offshore and river flow upstream. For the observation periods, the tidal record from the National Oceanic and Atmospheric Administration (NOAA) station at Boston (#8443970) was used as the boundary water surface elevation. River discharge data from the U.S. Geological Survey (USGS) gage at Lowell (#01100000) was multiplied by 1.1 to account for inputs below the gauging station. The depth-dependent, time-varying salinity at the offshore boundary was based on data from Gulf of Maine Ocean Observing System buoys in Massachusetts Bay (Buoy A) and on the Western Maine Shelf (Buoy B).

[12] FVCOM incorporates turbulence closure schemes through the General Ocean Turbulence Model (GOTM). GOTM is a 1-D vertical module that recasts various closure schemes in a uniform format [*Umlauf and Burchard*, 2003]. For the model to reproduce the strong pycnocline observed during high discharge conditions, it was important to set the background turbulent diffusivity to a small value (10^{-7} $m^2 s^{-1}$ in these simulations, but results were similar for 10^{-6} $m^2 s^{-1}$). Similarly, the subgrid scale horizontal diffusivity was set to zero to limit mixing of the sharp horizontal salinity gradients. Several turbulence closure schemes were tested. Most of the

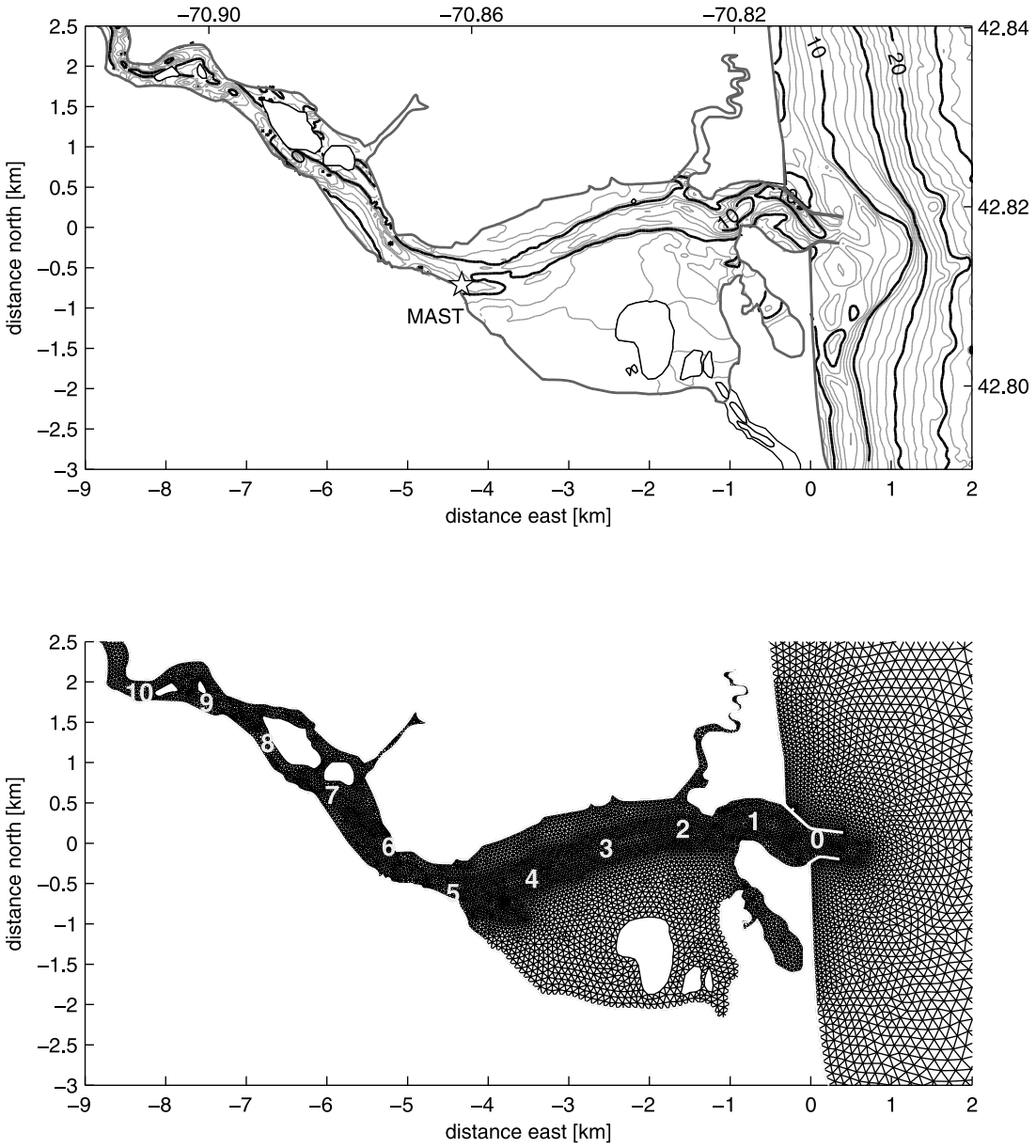

Figure 1. (top) Bathymetry for the Merrimack River estuary, including location of the MAST ebb anchor station measurements in 2007. (bottom) FVCOM model grid, indicating distance (km) from the mouth in the along-channel transects shown in Figures 2 and 3. Note this plot focuses on the estuary and that the full grid extends offshore from the mouth approximately 35 km to the north, east, and south, and up-river 25 km to the west.

results presented use the k-ε closure [*Rodi*, 1987] with stability coefficients from *Canuto et al.* [2001, version "A"], but we also consider k-ε with stability coefficients from *Kantha and Clayson* [1994] and the Mellor-Yamada level 2.5 closure [*Mellor and Yamada*, 1982].

[13] The model was calibrated by adjusting the bottom roughness (z_0) to match the tidal advection of the salinity intrusion from moored instruments in 2005. The same constant, uniform value of $z_0 = 0.5$ cm was used for simulations of the May 2007 observation period. The model results compared favorably with surveyed along- and across-channel distributions of salinity and velocity [see *Ralston et al.*, 2010, for details]. In addition to the realistic forcing, idealized simulations were run over the expected range of tidal and fluvial forcing for the Merrimack. Discharge ranged over seasonal low to high flows (25, 50, 100, 200, 400, 700, 1000, and 2000 $m^3\ s^{-1}$) and tides ranged from neap to spring amplitudes (2.0, 2.4, 2.8, and 3.2 m range).

[14] We consider when mixing occurs through the tidal cycle (flood-ebb asymmetry), where mixing occurs in the estuary (localized or distributed), what the dominant mechanisms for mixing are (bottom boundary layer or free shear layer turbulence), and how the mixing depends on forcing (spring-neap tides and river discharge). We use the model to calculate directly the mixing of momentum and salt. For momentum transfer in the water column, the

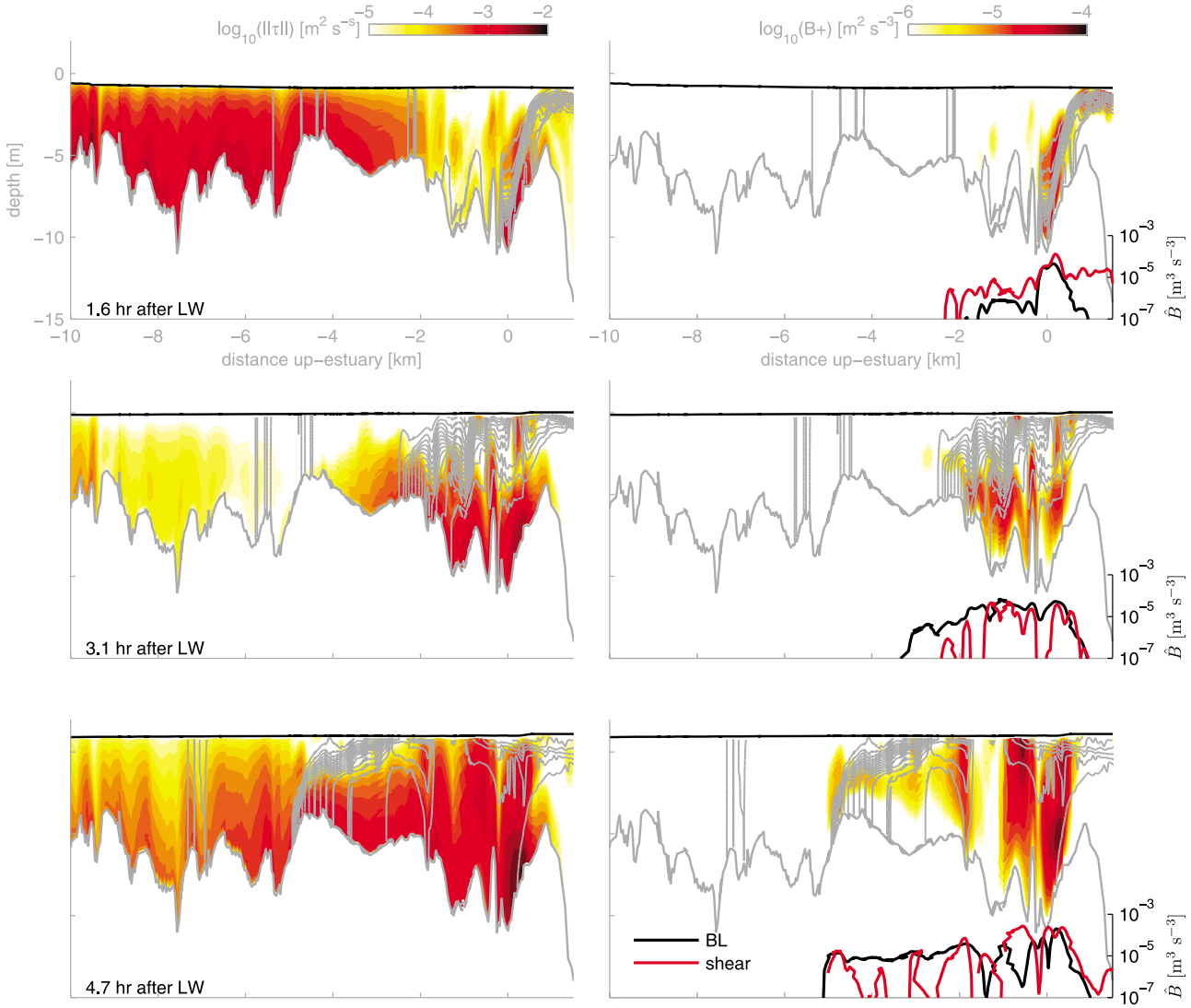

Figure 2. Along-channel snapshots of (left) shear stress and (right) instantaneous buoyancy flux during a flood tide. (Log scale, so B < 0 not shown). Salinity isohalines are shown in gray (every 2 psu). Model uses realistic forcing from observation period in 2005, and the case shown is from 29 May 2005 when Q_r was about 550 $m^3\ s^{-1}$ and tidal range was 2.8 m. The inset axes on the right show the partitioning of the depth integrated buoyancy flux in the channel between boundary layer turbulence and internal shear layer turbulence (as defined in section 3.2) at this instance.

magnitude of the shear stress is expressed as $\|\tau\| = \|(\overline{u'w'}, \overline{v'w'})\| = K_m[(\partial u/\partial z)^2 + (\partial v/\partial z)^2]^{1/2}$, where K_m is the eddy viscosity from the turbulence closure. The stress (or friction velocity) at the bed is $u_*^2 = C_d u_1^2$ where C_d is the drag coefficient and u_1 is the velocity at the lowest sigma level at distance z_1 from the bed. The drag coefficient depends on the bed roughness (z_0): $C_d = \left[\kappa/\ln\left(\frac{z_1 + z_0}{z_0}\right)\right]^2$. As in the model, this assumes a log layer velocity profile immediately above the bed. The buoyancy flux that mixes salt vertically is $B = \frac{g}{\rho_0}\overline{\rho' w'} = -g\beta K_h \partial s/\partial z$ where K_h is the eddy diffusivity and β is the coefficient of saline contraction ($\beta = 7.7 \times 10^{-4}$ psu^{-1}, with $\rho = \rho_0(1 + \beta\bar{s})$. We use buoyancy flux as a measure of the turbulent mixing of salt, but an alternative approach would be to calculate the decay in depth-integrated salinity variance [*Burchard et al.*, 2009]. The buoyancy flux is derived directly from the turbulence closure (K_h) and stratification, but the calculated mixing would be reduced by instances of convective mixing when $B < 0$. Generally the two approaches give similar results [*Burchard et al.*, 2009], but the treatment of convective instabilities in turbulence modeling remains an area of research and the use of scalar variance decay to assess mixing avoids this issue.

3. Results

3.1. Estuarine Buoyancy Flux

[15] For a section along the channel (location shown in Figure 1), we plot the shear stress and buoyancy flux at instances through the flood (Figure 2) and ebb (Figure 3)

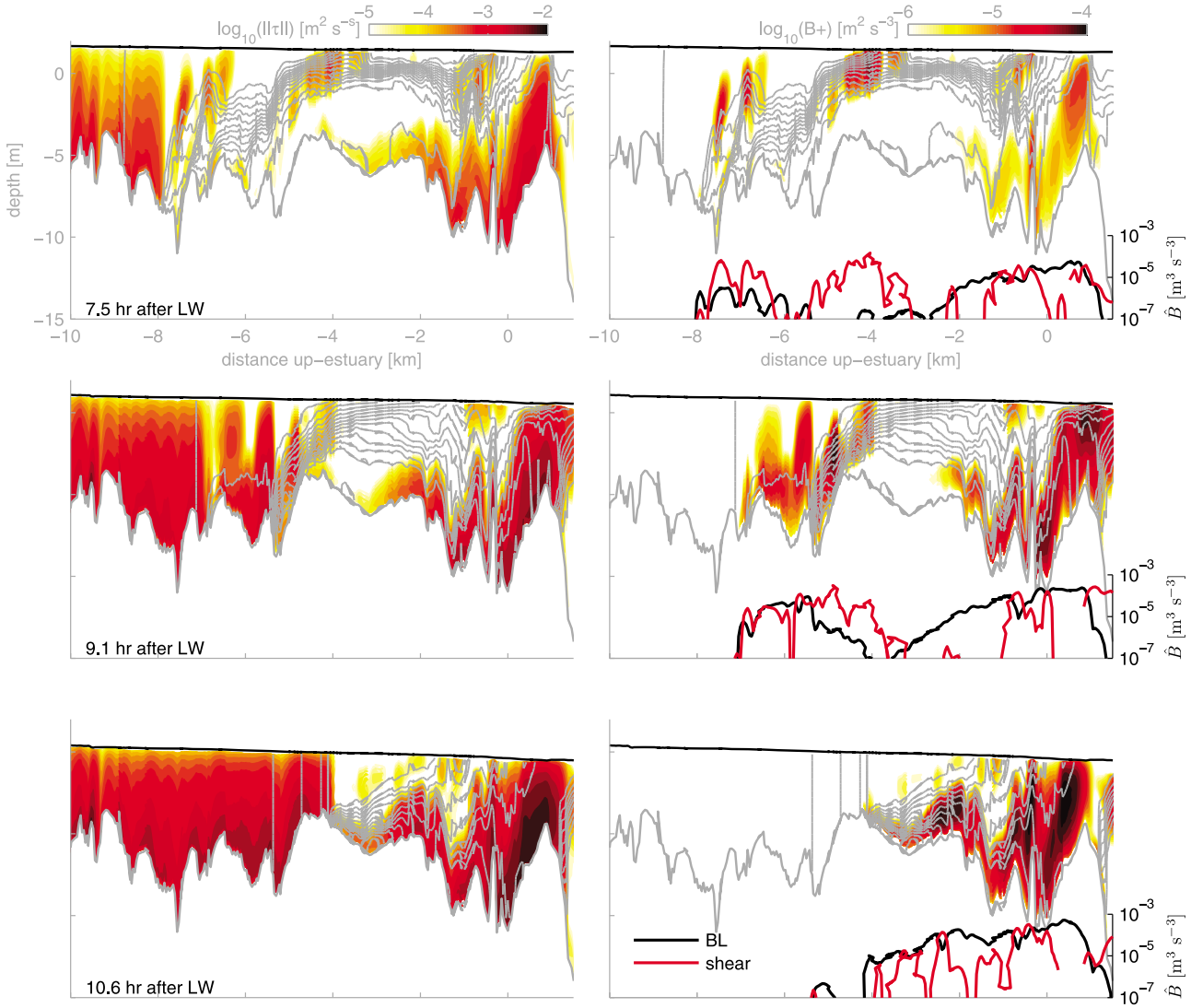

Figure 3. Along-channel snapshots of (left) shear stress and (right) buoyancy flux during an ebb tide. Salinity isohalines are shown in gray (every 2 psu). Model uses realistic forcing from observation period in 2005, and the case shown is from 29 May 2005 when Q_r was about 550 m^3 s^{-1} and tidal range was 2.8 m. The inset axes on the right show the partitioning of the depth integrated buoyancy flux in the channel between boundary layer turbulence and internal shear layer turbulence (as defined in section 3.2) at this instance.

together with the salinity isohalines. These snapshots were taken from a simulation of the observation period in 2005 when Q_r was about 550 m^3 s^{-1} and tidal range was 2.8 m. Tidal phases are noted as time since the previous low water (LW). Note that the tide in the Merrimack is essentially a standing wave, so tidal velocities are 90° out of phase with the water surface elevation.

[16] At the beginning of the flood tide, shear stresses are large in the fresh upper estuary, but without salinity gradients the buoyancy fluxes are near zero (Figure 2, 1.6 h after LW). As the salt wedge advances into the estuary, buoyancy flux occurs in the pycnocline as it passes through the narrow mouth region (along channel position −1 to 0.5 km). Later in the flood (4.7 h after LW), shear stresses are large throughout the region of salinity intrusion and are greatest near the bed, indicative of bottom boundary layer-generated turbulence. Buoyancy fluxes remain large in the mouth region, but farther up-estuary are comparatively weak in the pycnocline.

[17] Strong tides generate large shear stresses during the flood tide, but the mixing of salt is relatively ineffective for several reasons. During moderate to high river discharge, the water column during floods is highly stratified with an elevated pycnocline. The salinity gradient is physically separated from the source of turbulence at the bed (Figure 2, bottom), limiting the effectiveness of the bottom-generated turbulence. During floods the velocity maximum often coincides with the pycnocline, so the shear goes to zero near the maximum stratification, reducing the local turbulence production. Consequently, the buoyancy flux during floods (exclusive of the energetic mouth region) is small despite the significant tidal energy and vertical salinity gradients.

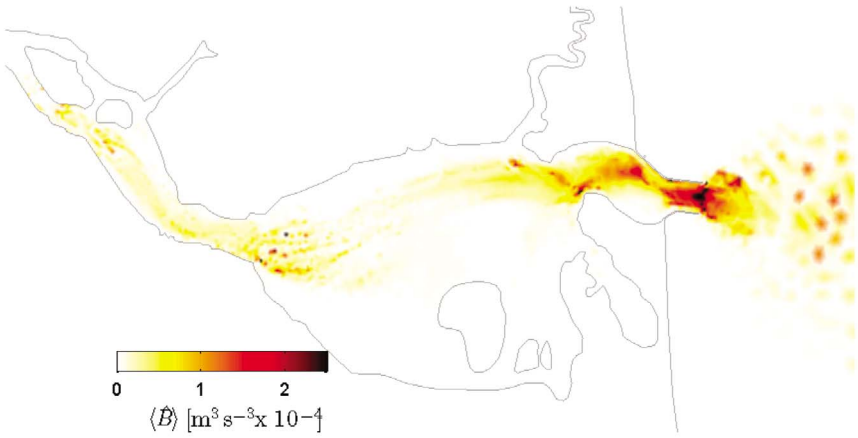

Figure 4. Depth-integrated, tidally averaged buoyancy flux for the period shown in Figures 2 and 3 (29 May 2005).

[18] During the early ebb (Figure 3, 7.5 h after LW), boundary-generated stresses occur in regions of weak stratification up-estuary, but several patches of elevated stress are also located in the pycnocline (along-channel position −7.5 km, −6.9 km, and −4.3 km). These regions of enhanced shear stress and mixing correspond with bathymetric sills and expansions. The mixing occurs mid water column and is distinct from bottom boundary layer turbulence. Later in the ebb, the stress and buoyancy flux at these locations becomes directly associated with bottom-generated turbulence (e.g., −4.3 km at 9.1 h after LW). As for the flood, the energetic mouth region has high stresses and buoyancy fluxes, particularly late ebb. As velocities intensify and the salt wedge breaks down (10.6 h after LW), the buoyancy fluxes increase and become more uniform along the channel from midestuary out the bar. Overall, the buoyancy flux in the estuary during the ebb is significantly greater than during the flood.

[19] The map of depth-integrated, tidally averaged buoyancy flux ($\langle \hat{B} \rangle$, with angle brackets for tidally averaged quantities and a hat for depth averaged) for the same tidal cycle illustrates the strong mixing in the mouth region but also shows lateral heterogeneity not apparent in the along-channel sections (Figure 4). Rock jetties at the mouth constrain the flow and create high velocities. Strong turbulence and secondary circulation due to the channel curvature induce mixing during both flood and ebb. Farther up-estuary the geometry is not as abrupt and constrained as at the mouth, and localized regions of intensified mixing are at the sills (−7.5 km and −6.9 km) and the sill and expansion onto the tidal flats (−4.3 km). The total mixing energy at these bathymetric transitions is less than at the mouth and bar, but it is substantial relative to the mixing at other locations in the estuarine interior.

[20] Outside the estuary, $\langle \hat{B} \rangle$ in the plume is patchier. The patchiness occurs as a result of small temporal and spatial fluctuations in gradient Richardson number that allow or suppress mixing according to the turbulence closure. The patchiness results in part from an undersampling of the model with output every 15 min rather than at every time step. A continuous time integration or longer averaging period would generate a more spatially uniform distribution of mixing in the offshore plume than this discrete sampling over a tidal cycle.

3.2. Mechanisms of Mixing: Internal Shear Versus Boundary Layer Mixing

[21] We now consider two different mixing mechanisms, one in which the mixing originates as instability of a shear layer and the other in which the turbulence is generated at the bottom boundary. Shear layer turbulence is most distinctive during the early to midebb when weak near-bottom currents and the baroclinic gradient (often associated with topographic transitions at sills and expansions) enhance shear across the pycnocline and lead to shear instabilities [*Geyer and Smith*, 1987]. Boundary induced mixing is the dominant mechanism in partially stratified estuaries [*Peters*, 1999], but it is also important in the highly stratified Merrimack. Boundary mixing is most effective when near-bottom currents are strong and the boundary layer is stratified.

[22] In the boundary layer, the maximum shear stress is near the bed and decreases with distance from the bed. For internal shear, the maximum stress occurs in the middle of the shear layer. At times, local maxima in shear stress exist simultaneously near the bed and in the upper water column. To quantify the relative contributions of boundary layer and shear layer mixing to the total buoyancy flux, we evaluate shear stress profiles in each grid cell at each output time step. Locations where shear stress decreases monotonically with distance above the bed are assigned entirely to boundary layer turbulence. Locations with a local minimum in stress middepth are divided between the processes, with mixing below the elevation of minimum stress attributed to boundary layer turbulence and above the stress minimum assigned to internal shear. This simulation (as well as the parametric studies described later) was for a period with negligible wind forcing, but to extend this approach to realistic simulations with wind stress would require similar separation between the surface boundary layer and internal shear.

[23] Using these definitions, the total buoyancy flux inside the estuary can be divided into boundary layer and shear

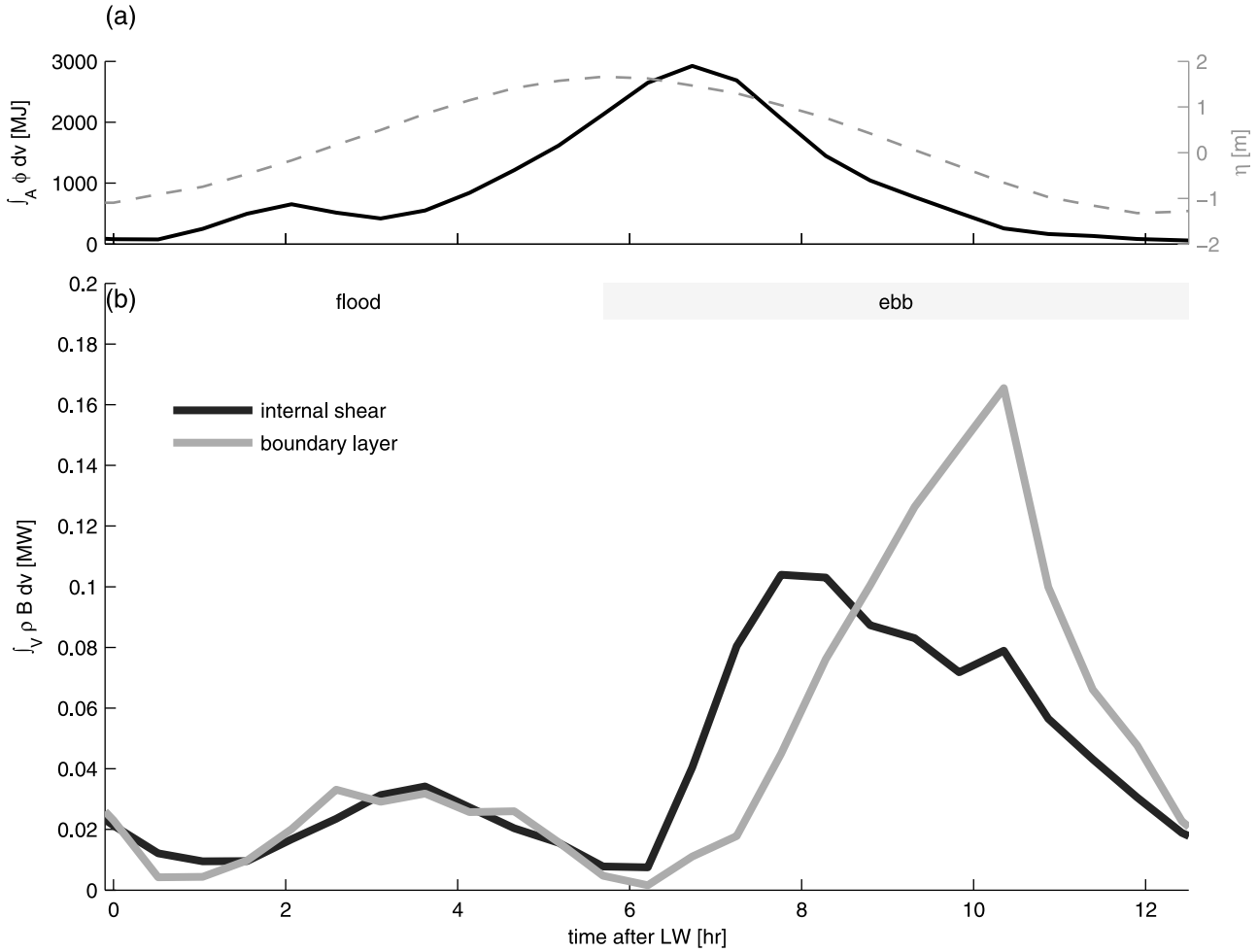

Figure 5. Time series of volume-integrated buoyancy flux in the estuary through a tide (same tidal period shown in Figures 2–4). (a) Water surface elevation (gray, right axes) and area-integrated (over the estuary) potential energy anomaly ϕ, a measure of the stratification in the estuary. (b) Volume integrated buoyancy flux times density in the estuary, divided between buoyancy flux due to bottom boundary layer and internal shear layer turbulence.

layer components and quantified through a tidal cycle. The along-estuary structure of the partitioning between shear and boundary layer buoyancy flux can be seen in depth integrated sections of $\hat{B}$ during flood (Figure 2) and ebb (Figure 3). Buoyancy flux can be multiplied by density and integrated over the volume of the estuary to arrive a time series for the total turbulent mixing in the estuary (Figure 5, same simulation period as Figures 2–4).

[24] During the flood, the volume-integrated buoyancy flux is relatively weak. Mixing is partitioned nearly equally between boundary layer and internal shear mechanisms. Lateral circulation during floods in the vicinity of the mouth creates vertical shear and turbulent mixing midwater column that is attributed to the internal shear mechanism, and bottom generated turbulence produces some mixing at the base of the pycnocline (Figure 2). Around high water slack buoyancy flux decreases. As the ebb begins, shear increases across the pycnocline while near-bottom velocities remain near zero and mixing is primarily due to internal shear (Figure 5). Later in the ebb, the bottom layer begins to move seaward, the pycnocline moves down in the water column, and boundary layer turbulence is the primary source of mixing. For these forcing conditions, the ebb accounts for about 80% of the total buoyancy flux. Over the tidal cycle, internal shear provides about 50% of the total mixing in the estuary with the rest due to boundary layer turbulence.

[25] Buoyancy flux requires stratification on which the turbulent kinetic energy can act. One measure of the stratification is the potential energy anomaly, the amount of mechanical energy needed to homogenize the water column for a given stratification [*Simpson et al.*, 1981]. The potential energy anomaly is $\phi = \frac{1}{H}\int_{-h}^{\eta}(\overline{\rho} - \rho)gz\mathrm{d}z$, where $\overline{\rho}$ is the depth-averaged density, η is the water surface elevation, and h is the distance to the bed relative to mean sea level, and $H = (\eta + h)$ is the total water depth. The area-integrated ϕ is indicative of the amount of stratification in the estuary through the tidal cycle (Figure 5) and is an upper bound on the amount of mixing that can occur. Through much of the flood, the potential energy anomaly is relatively low and constant as the salt wedge moves into the estuary. Around high water slack and early ebb (~6–8 h after LW),

the integrated ϕ increases substantially as the bottom layer continues to move up-estuary and the surface layer begins to ebb, increasing the area with strong stratification. During peak ebb, ϕ in the estuary decreases due to mixing and advection of stratification to the plume. The ϕ time series indicates that the enhanced mixing during ebbs depends in part on the increase in stratification created by expansion of the salt wedge around high water slack.

3.3. Dependence of Buoyancy Flux on Forcing

[26] We expect that the magnitude and mechanisms of estuarine mixing depend on the relative strengths of tidal and fluvial forcing. To quantify variability in mixing through parameter space we ran idealized cases with constant discharge and tidal amplitude. Cases included Q_r of 25, 50, 100, 200, 400, 700, 1000, and 2000 $m^3\ s^{-1}$ and tidal range η_0 of 2.0, 2.4, 2.6, and 3.2 m, reflective of the seasonal discharge and the spring-neap tidal variability in the Merrimack. Each case was run until conditions reached a tidally periodic steady state. The tidally averaged horizontal Richardson number ($Ri_x = g\beta(\partial s/\partial x)H^2/(C_d U_t^2)$) over the range of forcing conditions is shown (Figure 6a), but the Merrimack is highly variable and the temporal and spatial fluctuations in Ri_x are significant, particularly at higher Q_r. See *Ralston et al.* [2010] a more extensive discussion of how the Merrimack fits into estuarine parameter space.

[27] Over the range of discharge and tidal forcing conditions tested, we find that buoyancy flux in the estuary is always greater during ebbs than during flood tides (Figure 6b). Here we plot the volume-integrated buoyancy flux times density integrated over a tidal cycle to yield mixing energy. The greater mixing during ebbs depends in part on the stratification and ϕ created around high water (Figure 5). The tidal asymmetry in mixing is most notable at moderate to high discharge when integrated buoyancy flux during the flood is less than half of the mixing during the ebb. The mixing during flood tides is not enhanced by river discharge, but greater Q_r does increase shear and stratification during ebbs to produce greater total mixing, particularly at the breakdown of topographic fronts and at the mouth bar. River discharge increases the potential energy anomaly available to be mixed (Figure 6c). The tidally averaged, volume integrated ϕ in the estuary increases with Q_r except for the highest discharges where the river velocity is sufficiently strong to exclude salt water from the estuary for a large fraction of the tidal cycle. While the total buoyancy input (and thus potential energy anomaly) is greater for higher Q_r, more mixing is transferred offshore as the length of the estuary decreases.

[28] For the modeled observation period (Figure 5), internal shear mixing accounted for about half of the total buoyancy flux inside the estuary. Over the broader range of Q_r, this ratio varies from about 40% to 65% (Figure 7a, dashed lines). At lower discharges, the estuary becomes more weakly stratified and fronts are less likely to form at topographic transitions, while at higher discharges the horizontal and vertical salinity gradients intensify and the system becomes more frontal. The mixing mechanisms also depended on tidal amplitude; boundary layer mixing accounted for a greater proportion of the total buoyancy flux for stronger tides. Stronger tidal pressure gradients generate greater bed stress, thus increasing the relative contribution of the bottom boundary layer.

[29] The focus thus far has been on mixing processes inside the estuary, but freshwater that is not mixed in the estuary enters the plume and eventually mixes with the coastal ocean. Considering mixing more broadly to include the region offshore, the relative importance of internal shear grows substantially and depends more on Q_r (Figure 7a, solid lines). At higher discharges, low-salinity water exits the estuary and forms the plume. Most of the mixing in the plume occurs at the base of a thin surface layer separated from the bottom boundary layer by tens of meters of water. Bottom boundary mixing is substantial near the mouth where the flow accelerates over the bar and in shallow regions along the coast, but farther offshore the bottom stresses do not extend up to the stratification. For moderate to high discharge, internal shear is the primary mixing mechanism away from the bar and accounts for as much as 95% of the total mixing in the domain. A relatively small region where the plume spreads and decelerates offshore of the bar accounts for much of the plume mixing. For high discharge cases about 75% and for lower discharges about 45% of the total offshore mixing occurs within 2 km of the mouth.

[30] These idealized cases were run with zero wind stress. In reality, even moderate winds can create a surface boundary layer that contributes to mixing the plume. Simulations of the observational period that included surface wind stress had greater mixing in the offshore region than those without wind forcing. During periods of weak to moderate wind (wind speed <4 m s^{-1}), total buoyancy flux in the offshore region was 1.5–4 times greater than without wind. For periods with stronger winds (>4 m s^{-1}), total buoyancy flux offshore increased by a factor of 10 to 20 over the no-wind case. Wind mixing of the plume is important for plume fate and deserves additional consideration, but internal shear instabilities near the lift-off remain critical to the creation of the near-field plume.

[31] We quantify the total amount of mixing energy as volume integrals of buoyancy flux (multiplied by density) inside the estuary and in the estuary and coastal ocean integrated over a tidal cycle (Figure 7b). In both cases, the integrated buoyancy flux increases with tidal amplitude, as there is greater tidal energy available for mixing. Mixing both inside and outside the estuary also depends on Q_r, but with different functional forms. Inside the estuary, mixing increases with Q_r due to the greater density anomaly (or potential for mixing) supplied by the river, but only up to a point. Above about 400 $m^3\ s^{-1}$ the total mixing in the estuary decreases as the estuary becomes shorter and water exiting the mouth fresher. The low-salinity water that does not mix inside the estuary eventually mixes offshore, so the total buoyancy flux increases monotonically with Q_r. At 50 $m^3\ s^{-1}$ about 80% of the mixing occurs inside the estuary, at 2000 $m^5\ s^{-1}$ about 95% is outside the estuary, and the two regions have roughly equal mixing around 400 $m^3\ s^{-1}$.

3.4. Mixing Efficiency

[32] Variability in the mechanisms for mixing through parameter space should result in variability in the mixing efficiency. The flux Richardson is defined as $R_f = B/P$,

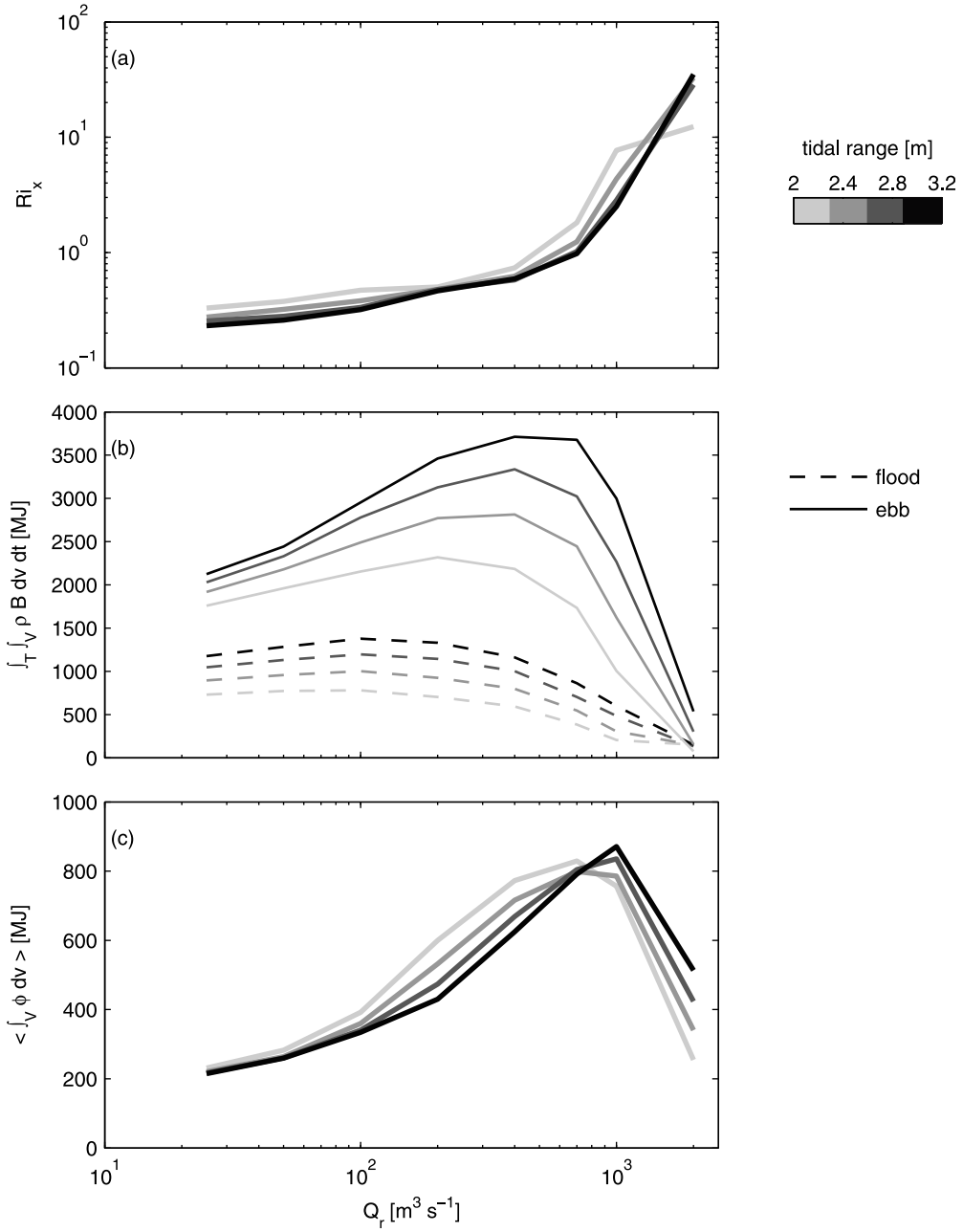

Figure 6. Mixing in the estuary during flood and ebb over a range of river and tidal forcing conditions. (a) Tidally averaged horizontal Richardson number in the estuary as a function of river discharge and tidal amplitude (line shading indicates tidal range from 2.0 to 3.2 m). (b) Volume integrated (over the estuary) buoyancy flux in the estuary, with dashed lines for integrated buoyancy flux over the flood tide while solid lines are for integrated buoyancy flux during ebb. (c) Volume integrated, tidally averaged potential energy anomaly ϕ. Note that instantaneously ϕ can be much larger as in the example period in Figure 5 ($Q_r \approx 550$ m^3 s^{-1}, $\eta \approx 2.8$ m).

where B is the buoyancy flux and P is the shear production $P = -\overline{u'w'}(\partial u/\partial z) - \overline{v'w'}(\partial v/\partial z)$. The expected maximum efficiency is R_f between 0.15 and 0.2 based on oceanic turbulence measurements and numerical simulations [*Ellison*, 1957; *Osborn*, 1980; *Ivey and Imberger*, 1991; *Shih et al.*, 2005]. R_f is 0 in the absence of stratification, and can be negative in the case of unstable stratification (convection).

[33] Field observations have found R_f from nearly 0 to greater than the theoretical maximum. In strongly stratified estuaries and plumes where internal shear mixing was the dominant source of buoyancy flux, R_f approached maximum efficiency. Examples include the mouth of the Fraser River

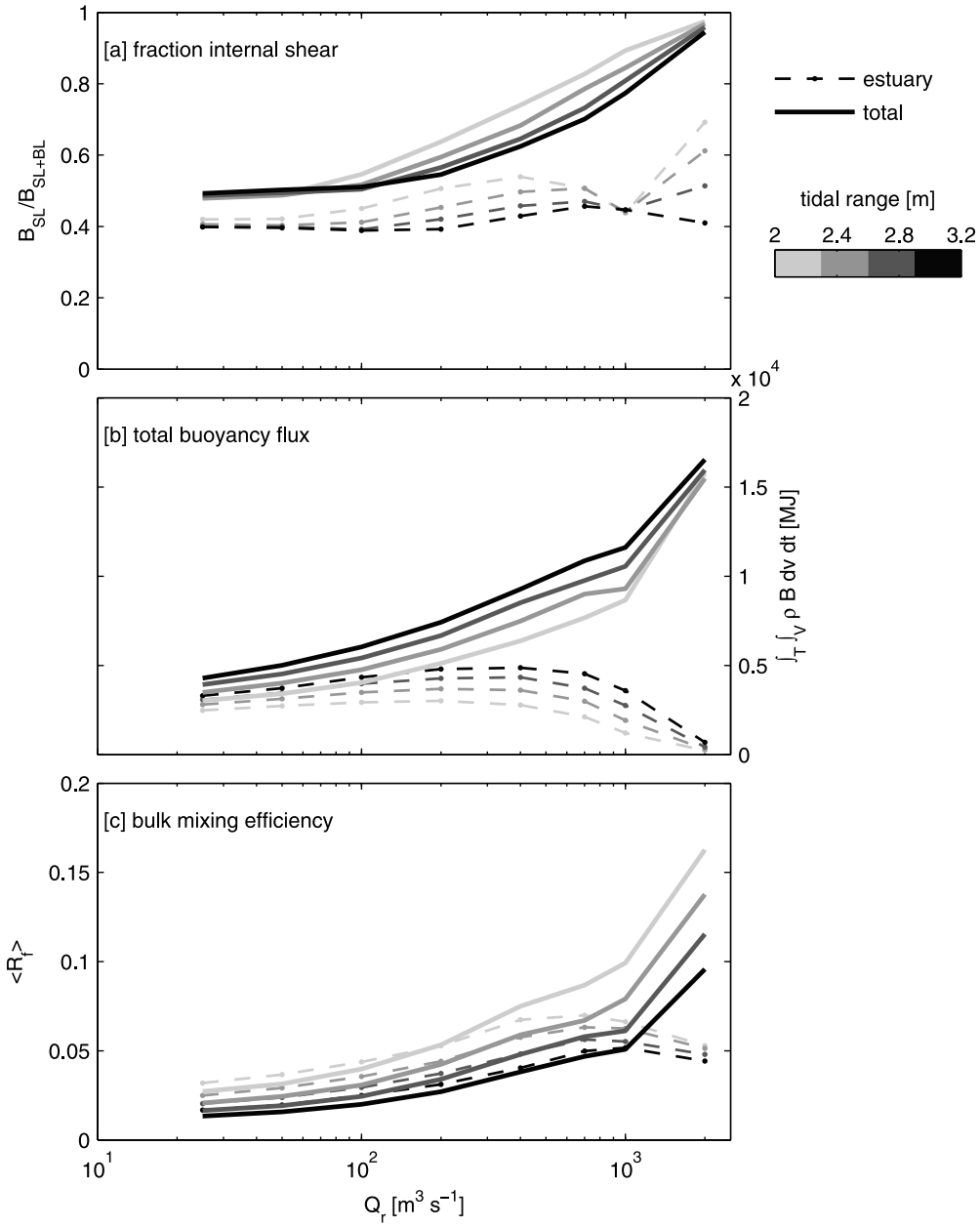

Figure 7. Dependence of mixing on river discharge and tides. Line shades indicate tidal range from 2.0 to 3.2 m. Dashed lines represent mixing inside the estuary while solid lines include the plume region offshore. (a) Fraction of the volume integrated (for each region, the estuary and the entire domain), tidally integrated buoyancy flux due to internal shear layer turbulence. (b) Volume-integrated, tidally integrated buoyancy flux. (c) Tidally averaged, bulk mixing efficiency (R_f) based on the ratio of volume integrated, tidally integrated buoyancy flux to volume integrated, tidally integrated turbulent shear production in each region.

with R_f between 0.15 and 0.25 [*MacDonald and Geyer*, 2004], the Columbia River salt wedge with R_f between 0.18 and 0.26 [*Kay and Jay*, 2003], and the Merrimack River plume with R_f around 0.2 [*MacDonald et al.*, 2007]. In an estuarine channel of San Francisco Bay, efficiencies near the bed were low (0.01–0.05) where shear production was intense but the stratification and buoyancy flux were weak [*Stacey et al.*, 1999]. Closer to the pycnocline, stratification increased, shear production decreased, and R_f increased to around 0.2. Similarly, bottom boundary layer mixing during flood tides in the Hudson River estuary was less than maximal efficiency, with R_f between 0.1 and 0.18 [*Chant et al.*, 2007]. Boundary-layer mixing can be extremely inefficient in regions with strong tides and weak stratification, such as on the continental shelf where efficiency was estimated at 0.004 [*Simpson and Bowers*, 1981].

[34] In the Merrimack, observations with the MAST at an anchor station (Figure 1) during two ebb tides indicated that

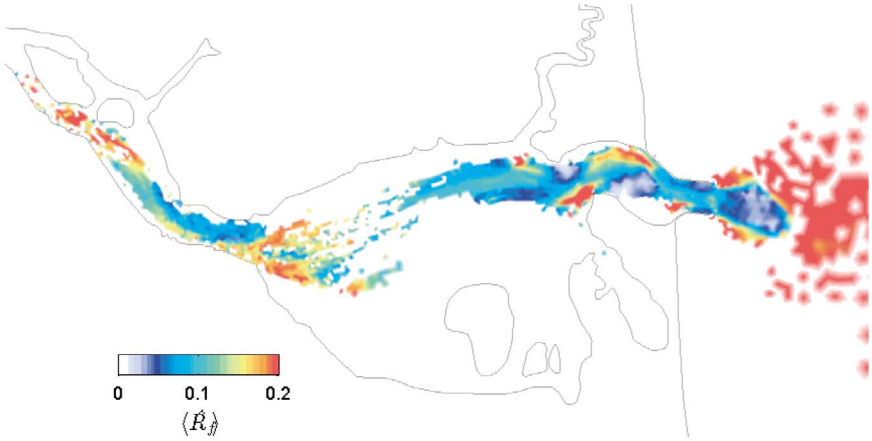

Figure 8. Spatial distribution of tidally averaged flux Richardson number (depth-integrated, tidally integrated buoyancy flux divided by depth-integrated, tidally integrated shear production over the tidal cycle shown in Figures 2–5).

R_f varied between 0.05 and 0.3, and almost half of the measurements had $R_f > 0.15$ [*Geyer et al.*, 2008]. The variability within the observations in part depended on changing conditions during the ebb, from shear instabilities high in the water column early in the ebb (and high R_f) to bottom generated turbulence acting on weaker stratification (with lower R_f) late in the ebb. With the model, we evaluate how the mixing efficiency depends on the tidal and river forcing.

[35] The bulk mixing efficiency in the model is calculated as the ratio of the tidally integrated, volume integrated buoyancy flux to the tidally integrated, volume integrated shear production: $\langle R_f \rangle = \int_T \int_V B \mathrm{d}v\mathrm{d}t \Big/ \int_T \int_V P \mathrm{d}v\mathrm{d}t$ with the volume integral limited to the region with salt (>0.5 psu). The bulk mixing efficiency inside the estuary and in the entire domain depends on the relative contribution of internal shear mixing to the total buoyancy flux (Figure 7c). At low Q_r, boundary layer mixing is greater and mixing efficiencies are low, between 0.015 and 0.03. The bulk efficiency depends on tidal amplitude, with more efficient mixing during weaker tides, again consistent with the proportional contribution of internal shear layers. $\langle R_f \rangle$ increases with discharge as the system becomes more stratified and frontal. The maximum average efficiency in the estuary is about 0.07, less than half of the theoretical maximum. Considering the entire domain the average efficiency increases substantially, as shear layer mixing at the base of the plume accounts for a greater fraction of the total. At $Q_r = 2000$ m^3 s^{-1} and 2.0 m tidal range, the domain average mixing efficiency is about 0.16, indicating the predominance of shear-induced mixing in the plume offshore of the mouth. Note that the steady state gradient Richardson number (Ri_{st}) value of R_f (the R_f at which turbulence approaches equilibrium in homogeneous shear layers) in the k-ε closure depends on the value chosen for the stability parameter c_3 [*Burchard and Hetland*, 2010]. In the *Canuto et al.* [2001] formulation, c_3 depends on the prescribed Ri_{st}, set here at 0.25 with the resulting efficiency at steady state of $R_f = 0.188$.

[36] The mixing efficiencies calculated in the model are generally lower than observed with the MAST, but the model results may be more representative of average conditions in the estuary. The MAST did not reach near the bed because of operational limitations, so it did not measure turbulence or mixing in this region of high shear production and relatively weak stratification. The model results indicate that roughly 1/3 of the shear production in the estuary occurs due to stress at the bottom boundary. The near-bottom turbulence is relatively inefficient without stratification to work against, and the MAST is likely to overestimate R_f because it misses this region.

[37] The model results also indicate substantial spatial heterogeneity in mixing efficiency due to the bathymetry and mixing mechanisms (Figure 8). Depth-averaged, tidally averaged mixing efficiencies approach the theoretical maximum offshore in the plume and at the sills and expansions that have significant interfacial shear mixing during ebbs. Efficiencies are much lower in the mouth and over the bar where boundary layer turbulence is intense but a lower fraction of the turbulent energy results in buoyancy flux. As with buoyancy flux, the bulk efficiency varies laterally with the bathymetry and dominant flow patterns. In contrast, observations from the MAST sampled a single location with relatively high R_f due to internal shear mixing downstream of a topographic transition. Field measurements in other estuaries would have similar limitations in spatial and temporal coverage that may bias estimates of mixing efficiencies high.

[38] The bulk mixing efficiencies calculated for the Merrimack estuary and the plume are comparable to those from a model of the Columbia River estuary under moderate discharge conditions ($Q_r \sim 4000$ m^3 s^{-1}, annual mean $Q_r \sim 7500$ m^3 s^{-1}), where R_f averaged in the plume region was 0.17 and averaged in the estuary was 0.05 [*MacCready et al.*, 2009]. Here we show that the mixing efficiency de-

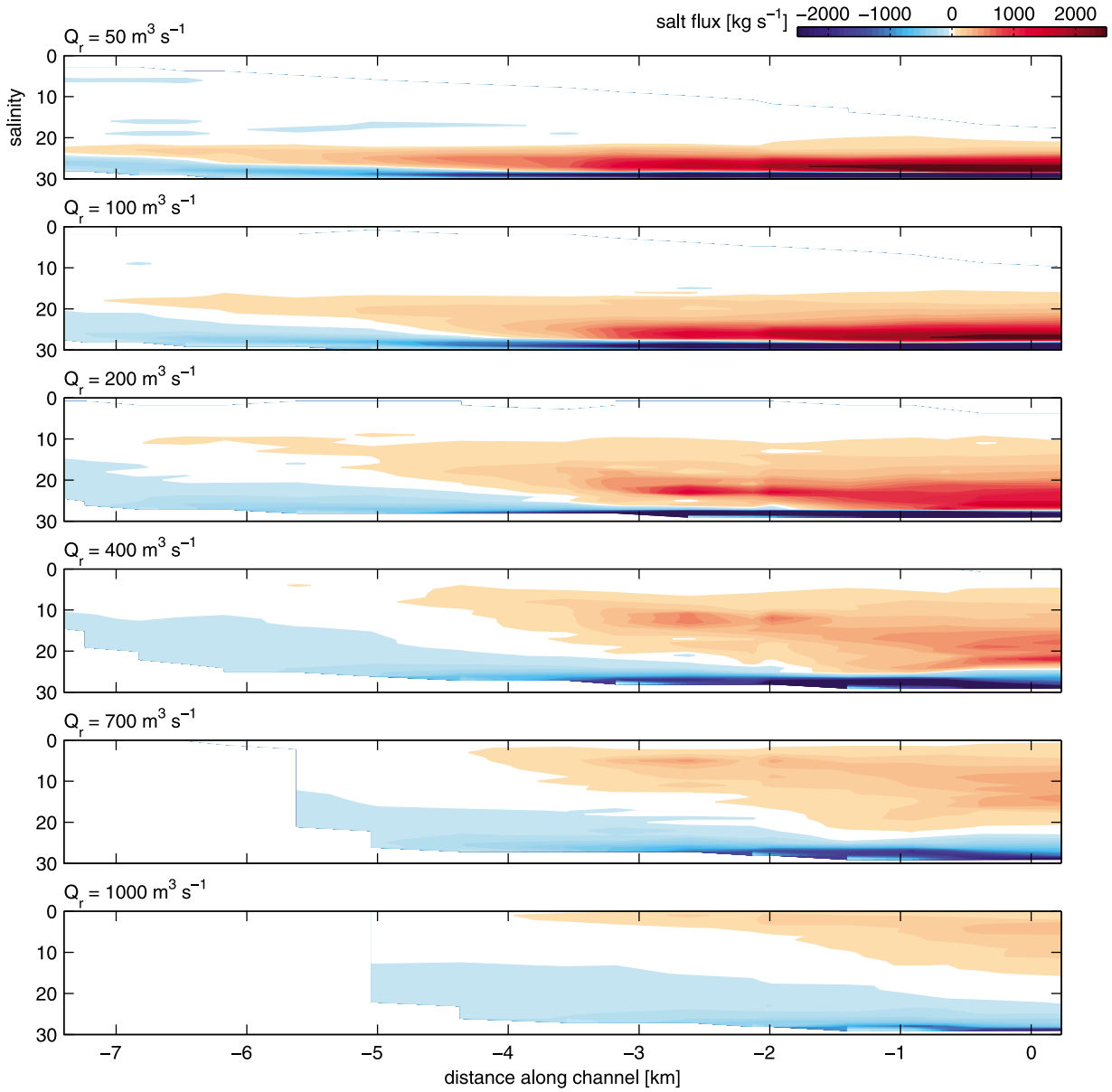

Figure 9. Net advective salt flux binned by salinity class for different river discharges. At cross sections along the estuary, salt flux up-estuary and down-estuary are divided into salinity classes between 0 and 30. The difference between the up-estuary and down-estuary fluxes is contoured as a function of distance from the mouth.

pends on Q_r, tidal amplitude, and the mechanisms of mixing, and the same is likely true of the Columbia.

3.5. Locally Intensified Mixing

[39] Whether by boundary layer or internal shear layer turbulence, mixing of salt and freshwater in the estuary transforms water properties. To evaluate where these water mass transformations occur along the estuary, we divided the advective salt flux into and out of the estuary into salinity classes [*MacDonald and Horner-Devine*, 2008]. At cross sections along the channel axis separated by about 400 m, we sorted the advective salt flux into salinity bins between 0 and 30 psu. The net salt flux or difference between the up-estuary and down-estuary salt fluxes is shown as a function of distance along the estuary for different discharges (Figure 9). Cool colors correspond with salinity classes with net transport of salt (or oceanic water properties) into the estuary, and hot colors are salinity classes that have net transport down-estuary. The plots illustrate how salt moves through the estuary in physical (along-channel distance) and salinity space. Strong spatial gradients in net along-channel salt flux occur at locations of intensified mixing and transformation of water properties.

[40] For low discharges (e.g., 50 m^3 s^{-1}), salt moves up-estuary at nearly oceanic salinity (30 psu) and most of the salt exits the estuary only slightly fresher than it came in

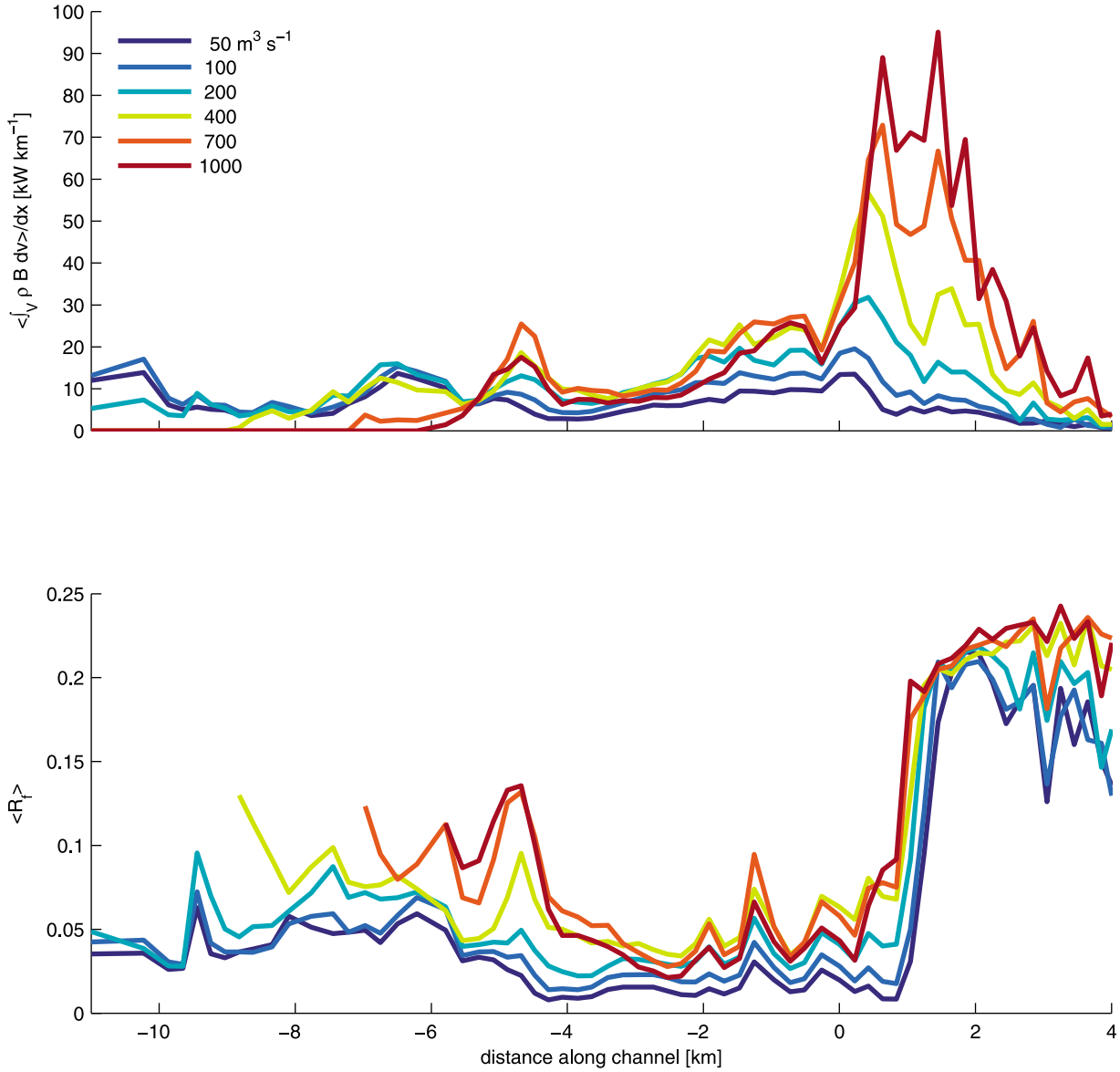

Figure 10. Buoyancy flux along the estuary for a range of river discharges. (top) Volume integrated, tidally averaged buoyancy flux summed in equally spaced bins (dx = 200 m) and normalized by bin width, plotted as a function of distance from the mouth. Line color indicates discharge, and all cases have tidal amplitude of 2.4 m. (bottom) Bin averaged bulk mixing efficiency (R_f) as a function of distance from the mouth, with R_f defined as the volume integrated, tidally integrated buoyancy flux divided by the volume integrated, tidally integrated shear production in each along-channel bin.

(~26–29 psu). The total mass of salt exchanged between the estuary and the coastal ocean is much greater than in high discharge cases and the total mixing energy is less, so the along-channel gradients in salt flux are weak. At higher discharges, the effects of localized mixing can be seen distinctly in the creation of lower salinity class water. At locations that correspond with regions of intensified ebb mixing (section 3.1, Figures 2 and 3), the net up-estuary salt flux in higher salinity classes decreases and the net down-estuary flux in lower salinity classes increases. As discharge increases, the separation in salinity space between incoming and outgoing salt increases. At 1000 m^3 s^{-1}, the net flux is up-estuary at nearly oceanic salinities, but much of that salt is returned to the coastal ocean at less than 10 psu.

[41] The spatial gradients in salt flux at moderate to high discharge indicate that a few regions of topographic transition disproportionately contribute to the total mixing and water mass transformation in the estuary. The buoyancy flux is integrated across the estuary and plotted as a function of distance from the mouth (Figure 10). Despite different total magnitudes of the buoyancy flux, specific locations along the estuary consistently have greater mixing and enhanced mixing efficiency. Two mixing hot spots that were active across the full range of discharge were the sill and expansion around 4.3 km and the bar at the mouth (around 0.5 km). As

shown previously, the sill and expansion creates a salinity front that produces internal shear mixing early in the ebb and is destroyed by boundary layer mixing later in the ebb. The opposing baroclinic pressure gradient during ebbs creates greater shear across the pycnocline, reducing Ri_g and allowing for greater buoyancy flux. Correspondingly, the mixing efficiencies are enhanced at this location, particularly for moderate to high discharge. In contrast, the energetic boundary layer over the mouth bar is a major source of buoyancy flux but is relatively inefficient. Offshore in the plume where the mixing is disconnected from the bottom boundary layer, R_f increases substantially.

[42] The partitioning between a few locally intense regions of mixing and more uniformly and broadly distributed mixing has been considered in other estuaries. In the Fraser, another highly stratified estuary, mixing was most intense at a few constrictions during ebbs and was relatively weak during floods and far from hydraulic transitions [*Geyer and Farmer*, 1989]. Similarly, mixing was enhanced downstream of constrictions in the Tweed estuary [*Uncles and Stephens*, 1996] and the Duwamish estuary, where intermittent shear instabilities during ebbs accounted for more than 50% of the mixing over less than 20% of the tide [*Partch and Smith*, 1978]. In more weakly stratified estuaries, we may expect that mixing is more evenly distributed due to the greater importance of boundary mixing and lack of baroclinic fronts. However, model results for the weakly to partially stratified Chesapeake Bay found that a few regions contributed disproportionately to the total mixing energy, with 40% of the tidal dissipation concentrated at three constrictions and a headland [*Zhong and Li*, 2006]. In the Hudson, enhanced mixing downstream of a hydraulic transition was proposed as important to the total mixing [*Chant and Wilson*, 2000], but microstructure observations found only a modest (2–3 times) increase in turbulence downstream of the transition [*Peters*, 2003]. A conclusion from the microstructure observations was that mixing was broadly distributed in the Hudson, with the important caveat that the observations were made during relatively low discharge conditions (Q_r = 50–250 m^3 s^{-1}, annual mean $Q_r \sim$ 600 m^3 s^{-1}). With moderate to high discharge, mixing in the Hudson is more likely to be localized to topographic transitions as in highly stratified estuaries. In fact, observations in the lower Hudson at moderate discharge ($Q_r \sim 500$ m^3 s^{-1}) found elevated mixing due to hydraulic response downstream of a topographic feature [*Peters*, 1999].

3.6. Model Sensitivity

[43] These mixing calculations depend substantially on the ability of the numerical model to realistically simulate physical processes. On the basis of comparisons with salinity and velocity observations, the model achieves high skill reproducing circulation and stratification in the Merrimack [*Ralston et al.*, 2010]. While observed salinities and velocities intrinsically depend on turbulent mixing, we have far fewer in situ measurements of turbulence quantities such as shear stress, buoyancy flux, or dissipation to test mixing in the model directly. We use limited observations of turbulence quantities in the Merrimack to evaluate the sensitivity of the model to different turbulence closure schemes. We also evaluate how grid resolution affects calculated mixing and estuarine outflow.

3.6.1. Turbulence Closure

[44] The results presented thus far have used the k-ε turbulence closure with stability constants from [*Canuto et al.*, 2001] (version "A," as described in the work of *Burchard and Bolding* [2001]). To test the sensitivity of the results to the turbulence closure, we ran the model using k-ε with alternative stability constants [*Kantha and Clayson*, 1994] and with the k-kl turbulence closure [*Mellor and Yamada*, 1982]. The turbulence closures were implemented using GOTM with the option to compute buoyancy stability parameters (c_3 for the k-ε models, E_3 for Mellor-Yamada) based on a steady state gradient Richardson number of 0.25 [*Burchard*, 2001; *Umlauf and Burchard*, 2005].

[45] As others have found, Reynolds averaged properties like salinity, stratification, and velocity were relatively insensitive to the turbulence closure [*Warner et al.*, 2005; *Li et al.*, 2005]. The Merrimack simulations were sensitive to the background diffusivity, but as long as it was set to a small value (here 10^{-7} m^2 s^{-1}) the turbulence closures all produced similar salinities and velocities. Chesapeake Bay model simulations also showed that low background viscosity and diffusivity were more important to reproducing observed stratification than the closure [*Li et al.*, 2005]. The background diffusivity is meant to represent unresolved mixing processes (e.g., shear instabilities at scales smaller than the grid, mixing due to internal waves) or to aid in numerical stability. Setting physically plausible background diffusivity is particularly important in a shallow, stratified estuary like the Merrimack where strong salinity gradients can generate significant buoyancy flux even for low background K_h.

[46] To directly compare the model with turbulence data, we use measurements taken with the MAST during anchor stations over two different ebbs in May 2007. The array of velocity and conductivity sensors provided buoyancy flux measurements at multiple elevations in the water column (Figure 11). For details on the processing of the MAST data, see *Geyer et al.* [2008]. Simulations corresponding with the observations are shown for the k-ε turbulence closure with the *Canuto et al.* [2001] or *Kantha and Clayson* [1994] stability coefficients.

[47] The salinity fields (isohalines over the buoyancy flux contours) in the two simulations are nearly identical and neither is clearly preferable compared with the observations. Both simulations also have spatial and temporal distributions of buoyancy flux that are roughly consistent with the MAST data. The magnitude of the buoyancy flux and timing of mixing with respect to the passage of the salt front are similar in the model and the observations. Localized maxima in mixing occur in the pycnocline that are distinct from the bottom boundary layer early in the ebb and later in the ebb the greatest buoyancy fluxes are close to the bottom boundary. Note that operationally the MAST has limited coverage near-surface and near-bottom, so measurements were not available in these key regions. While these initial comparisons are promising, more extensive time series over a broader range of conditions and more complete vertical coverage are needed for a rigorous field test of turbulence closures.

[48] Histograms of buoyancy flux as a function of Ri_g provide an overall comparison between the observations and the model (Figure 12). Model results are extracted to com-

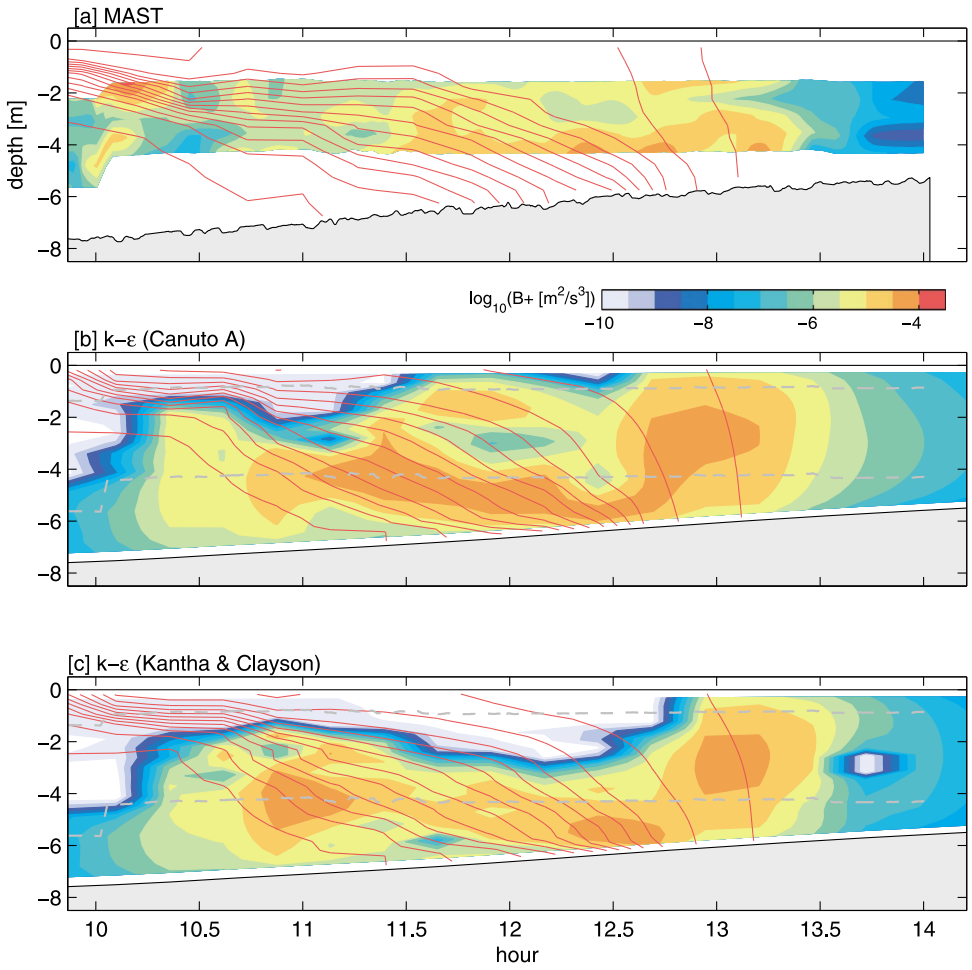

Figure 11. Buoyancy flux through an ebb tide at an anchor station (location in Figure 1, time is hour of 12 May 2007). Salinity contours are overlaid (every 2 psu). (a) Observations with the MAST. (b) Model results using k-ε closure with stability constants from *Canuto et al.* [2001, version "A"]. (c) Model results using k-ε closure with stability constants from *Kantha and Clayson* [1994]. The vertical extent of the MAST measurements is shown with dashed lines over the model results.

pare with the temporal and spatial coverage of the MAST. In the MAST data, mixing is roughly centered on the critical Ri_g of 0.25, with 90% of the buoyancy flux between $Ri_g \sim 0.1$ and 0.6. The two k-ε closures have similar distributions of buoyancy flux with Ri_g. Canuto A produces slightly greater mixing at $Ri_g > 0.25$ than Kantha and Clayson, but it is difficult to select one as preferable with respect to the observations. The tidally averaged, volume integrated buoyancy flux for each simulation is indicated on the plots. The total mixing with the Kantha and Clayson is about 6% less than with Canuto A.

[49] For comparison, we also show the buoyancy flux distribution with Ri_g for the Mellor-Yamada 2.5 closure [*Mellor and Yamada*, 1982]. Mellor-Yamada solves for turbulent kinetic energy (k) as in the k-ε closure, but rather than dissipation (ε), the second term in Mellor-Yamada is a turbulent length scale multiplied by the turbulent kinetic energy (kl). Mellor-Yamada suppresses mixing at high Ri_g, and comparisons with estuarine observations have found that it underestimates turbulent kinetic energy in strong stratification [*Stacey et al.*, 1999]. In comparison with the MAST data, Mellor-Yamada confines mixing to lower Ri_g than was observed. The total mixing in the estuary is substantially lower than for either of the k-ε closures. On the basis of the discrepancy between Mellor-Yamada and the observed Ri_g distribution of buoyancy flux we selected of the k-ε closure for these simulations.

3.6.2. Grid Resolution

[50] These results indicate that in highly stratified estuaries turbulent mixing is localized to topographic hot spots like sills and expansions. To resolve the mixing, the numerical model must resolve the bathymetric features that generate the shear and stratification. To test dependence on grid resolution, we ran equivalent cases using a lower resolution mesh. The horizontal grid spacing in the low resolution mesh was about 4 times that of the base case, and the total number of elements decreased from 23,507 to 1691. The vertical discretization of 20 sigma levels was kept constant. When cases were run to equilibrium, the lower resolution grid produced salinity intrusion lengths that were similar to those with the base case grid. While this implies that the lower resolution grid captures bulk attributes of the

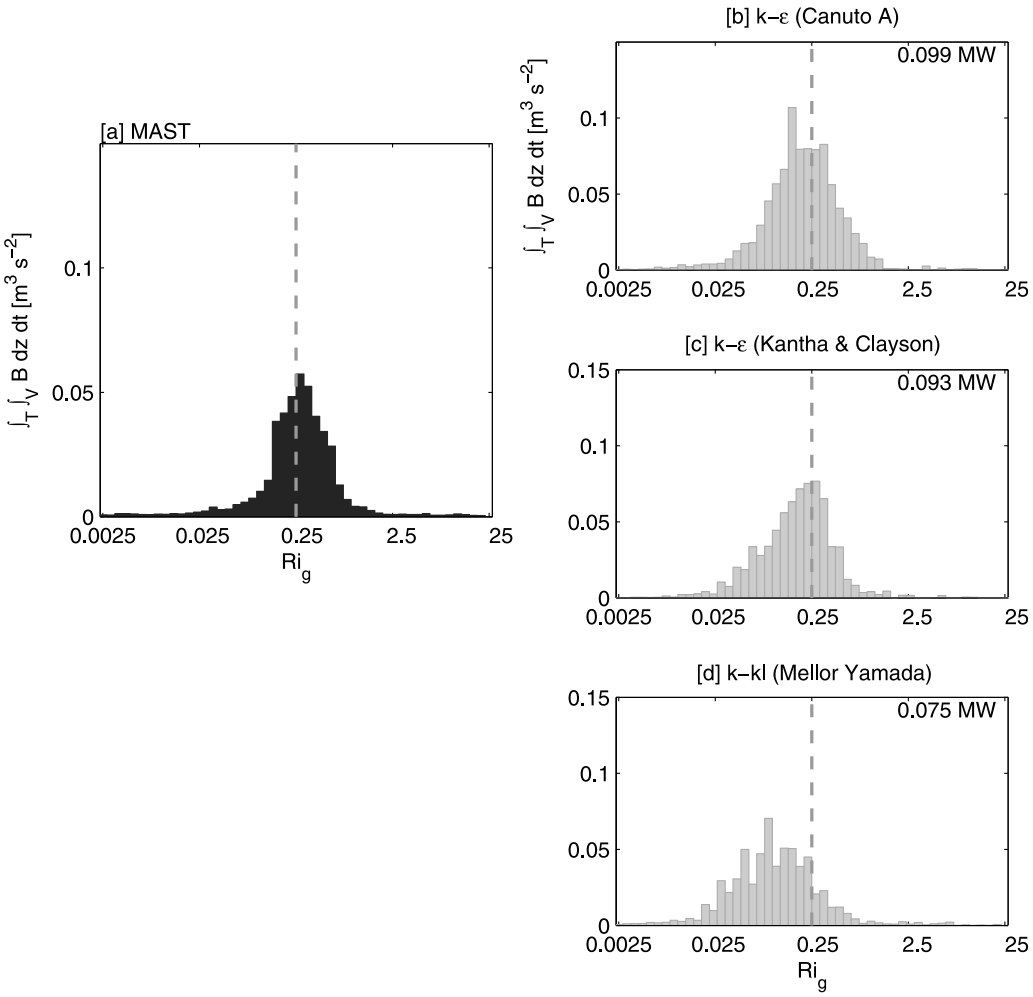

Figure 12. Buoyancy flux as a function of gradient Richardson number (Ri_g) from an anchor station (same location as Figure 11). Buoyancy fluxes are binned by Ri_g and integrated in z and time. Data shown are from ebb tides on 11 and 12 May 2007. (a) MAST observations. (b) Model results using k-ε closure with stability constants from *Canuto et al.* [2001, version "A"]. (c) Model results using k-ε closure with stability constants from *Kantha and Clayson* [1994]. (d) Model results using the *Mellor and Yamada* [1982] closure.

estuary, a more detailed examination indicates that the lower resolution grid calculates significantly less turbulent mixing. For given tidal amplitude, the integrated buoyancy flux inside the estuary with the lower resolution grid decreases by about 40% compared with the base case, and the decrease over the entire domain is as much as 30%, particularly at high discharges.

[51] For consistency, the bottom friction (z_0) for the coarser grid was set equal to that of the base case, but the optimal z_0 likely depends on grid resolution. Simulations of the observation period over a range of z_0 suggest a slightly lower roughness of z_0 of 1–2 mm provides higher model skill than with the base z_0 of 5 mm. A decreased z_0 is consistent with additional numerical mixing in the coarser grid (discussed below) that provides a momentum sink that compensates for reduced bottom friction. Coarse grid simulations with lower z_0 have even lower total buoyancy flux in the estuary and greater discrepancy in calculated mixing between the coarse and fine resolution cases.

[52] The vertical resolution of 20 sigma levels was selected based on comparison with observations of stratification in the estuary. Increasing the vertical resolution to 30 sigma levels did not improve the skill for salinity or stratification, and the total mixing in the estuary changed only slightly. For simulations of the 2005 observations (Figures 2–5), the volume integrated buoyancy flux in the estuary decreased by 3% when vertical resolution increased to 30 levels. The added vertical levels did permit better resolution of mixing at the base of the plume offshore, and the integrated buoyancy flux offshore increased by nearly 20%. While the model appears to be vertically well-resolved in the estuary and near the plume lift-off, the far-field mixing requires additional vertical resolution near-surface. In the far-field plume, wind is likely the dominant source of mixing, so model results also depend on accurate offshore wind data.

[53] An important difference between the coarse and base models may be the relative contribution of numerical mixing. Numerical mixing due to discretization errors in the advection scheme depends on flow velocity, scalar gradients, and grid resolution and can be equal to or greater than the mixing generated by the turbulence closure [*Burchard and Rennau*, 2008]. An evaluation of the numerical mixing in a coastal model found that the numerical mixing was greater than the turbulent mixing in regions with high velocities and strong horizontal scalar gradients [*Rennau and Burchard*, 2009]. The numerical mixing was sensitive to grid resolution, decreasing as the number of vertical layers increased or horizontal grid spacing decreased. In the Merrimack, the coarser grid likely has greater numerical mixing, thereby reducing not only the horizontal salinity gradients but also the vertical salinity gradients and velocity shear and consequently reducing the buoyancy flux calculated in the closure. A more thorough evaluation is needed to quantify numerical mixing in models with structured and unstructured grids, and the method presented by *Burchard and Rennau* [2008] offers a promising tool to do so.

[54] The dependence of mixing on grid resolution has consequences for representing estuarine processes in regional or global circulation models. For example, grid discretization and smoothing for numerical stability may shift the distribution of mixing between coastal and estuarine regions. An estuary with insufficient resolution and lower mixing rates (including both turbulent and numerical mixing) would export fresher water to the coastal ocean and potentially alter coastal transport. In the lower resolution Merrimack grid, more water exits the mouth at lower salinities and the plume is fresher than in the higher resolution grid. A constraint on grid resolution is the availability of accurate bathymetry data on scales similar to the grid spacing. In the higher-resolution Merrimack model, skills improved when additional bathymetry data were collected where soundings were sparse in the region near the expansion and transition to intertidal flats 4.3 km from the mouth. An unstructured grid model of the Snohomish River estuary also demonstrated that bathymetric data density and quality can limit model performance at high grid resolutions [*Wang et al.*, 2009].

4. Summary and Discussion

[55] To summarize, turbulent mixing of salt in the Merrimack occurs predominantly during ebbs and is concentrated in regions of topographic transition. Strong horizontal density gradients produce strong baroclinic pressure gradients that reduce near-bottom velocities and shear stress. Early in the ebb, shear increases across the pycnocline and internal shear layer instabilities provide the dominant mechanism for buoyancy flux. Later in the ebb as the salt wedge advects down-estuary and stratification weakens, bottom boundary layer turbulence is the dominant source of turbulent mixing. The relative partitioning between the boundary layer and internal shear layer mixing depends on the discharge, with greater contributions from internal shear mixing at higher discharges. The total mixing that occurs in the estuary also depends on discharge, with total buoyancy flux increasing up to about 400 $m^3\ s^{-1}$. At higher discharges, the estuary becomes so short that mixing inside the estuary decreases, and most of the mixing occurs offshore in the plume.

[56] The efficiency of the mixing depends on the partitioning between boundary layer and internal shear layer turbulence, varying with river discharge, and to lesser extent, tidal amplitude. Average mixing efficiencies in the estuary ranged between 2% and 7% from low to high discharge. Average efficiencies were as high as 16% including the offshore plume at high discharge. Buoyancy fluxes calculated from the model depended on the horizontal grid resolution and on the turbulence closure. A lower resolution model grid yielded less turbulent mixing (but likely increased numerical mixing) in the estuary and fresher flux out the mouth. The k-ε turbulence closure was most consistent with observed buoyancy fluxes and produced more total mixing than the Mellor-Yamada closure. More direct comparisons between observed and modeled turbulent quantities are necessary to rigorously evaluate turbulent closures. While bulk salinities and velocities in the estuary were relatively insensitive to changing turbulence closures, models of sediment transport, water quality, and physical-biological interactions are more likely to depend on details of turbulence and mixing.

[57] Modeling and observations have shown that the physical and temporal partitioning of mixing in partially mixed estuaries may be different than in the Merrimack. Simulations of an idealized partially mixed estuary showed that while the most intense mixing occurred during ebbs, more total buoyancy flux occurred during floods because the mixing was more prolonged and over a larger area [*MacCready and Geyer*, 2001]. Observations in the Hudson River estuary have been consistent with this view, that while buoyancy flux may be most intense during ebbs, the bulk of the mixing occurs through growth of the boundary layer during flood tides [*Peters*, 1999; *Chant et al.*, 2007]. By comparison in the Merrimack, the ebb accounted for between 65% of the total buoyancy flux at low discharge (Q_r = 25 $m^3\ s^{-1}$) and 85% at high discharge (1000 $m^3\ s^{-1}$).

[58] Deeper, longer estuaries like the Hudson exhibit significant variability in salinity intrusion length and mixing over a spring-neap cycle. During neap tides mixing is weak, baroclinic circulation and stratification are strong, the salinity field expands up-estuary and the total buoyancy flux is low. Stratification grows until spring tides when increased velocities mix away stratification and the salinity intrusion retreats down-estuary. In the more strongly forced Merrimack, mixing and salinity intrusion are less sensitive to the spring-neap cycle. Ebb tidal straining produces stratification in the Merrimack as in partially stratified estuaries, but depths are sufficiently shallow and tidal velocities are sufficiently strong to mix away stratification each tidal cycle rather than growing through a series of neap tides.

[59] Over the expected range of forcing, conditions in the Merrimack vary more with discharge than with tidal amplitude. Internal shear mixing is most important for moderate to high-discharge conditions when the salinity intrusion is pushed to the mouth bar at the end of each ebb. Stratification is created at the mouth bar and advects into the estuary with little mixing during the flood. The strong baroclinic pressure gradient and stratification interact to promote internal shear mixing early in the ebb followed by boundary layer mixing as the salt wedge breaks down. At

lower discharges, the salinity intrusion becomes longer than a tidal excursion and the front at the mouth bar is less significant. The more weakly stratified conditions during low discharge in the Merrimack appear similar to many partially mixed estuaries. However, the mixing remains ebb dominant and spatially heterogeneous even during low discharge conditions, distinct from the typical schematic for partially mixed estuaries that relatively uniform stratification is created during ebbs and mixed by boundary layer turbulence during floods. These realistic numerical simulations have demonstrated the spatial and temporal variability inherent in shallow, stratified estuaries, but additional modeling (in conjunction with field observations) is needed to quantify such processes in partially stratified estuaries.

[60] **Acknowledgments.** This research was funded by National Science Foundation Grant OCE-0452054. Ralston also received support from *The Penzance Endowed Fund in Support of Assistant Scientists* and *The John F. and Dorothy H. Magee Fund in Support of Scientific Staff* at Woods Hole Oceanographic Institution.

References

Burchard, H. (2001), On the q2l equation by Mellor and Yamada (1982), *J. Phys. Oceanogr.*, *31*, 1377–1387.

Burchard, H., and K. Bolding (2001), Comparative analysis of four second-moment turbulence closure models for the oceanic mixed layer, *J. Phys. Oceanogr.*, *31*, 1943–1968.

Burchard, H., and R. D. Hetland (2010), Quantifying the contributions of tidal straining and gravitational circulation to residual circulation in periodically stratified tidal estuaries, *J. Phys. Oceanogr.*, *40*, 1243–1262.

Burchard, H., and H. Rennau (2008), Comparative quantification of physically and numerically induced mixing in ocean models, *Ocean Modell.*, *20*, 293–311.

Burchard, H., F. Janssen, K. Bolding, L. Umlauf, and H. Rennau (2009), Model simulations of dense bottom currents in the Western Baltic Sea, *Cont. Shelf Res.*, *29*, 205–220.

Canuto, V. M., A. Howard, Y. Cheng, and M. S. Dubovikov (2001), Ocean turbulence: Part I. One-point closure model—Momentum and heat vertical diffusivities, *J. Phys. Oceanogr.*, *31*, 1413–1426.

Chant, R. J., and R. E. Wilson (2000), Internal hydraulics and mixing in a highly stratified estuary, *J. Geophys. Res.*, *105*(C6), 14,215–14,222, doi:10.1029/2000JC900049.

Chant, R. J., W. R. Geyer, R. Houghton, E. Hunter, and J. Lerczak (2007), Estuarine boundary layer mixing processes: Insights from dye experiments*, *J. Phys. Oceanogr.*, *37*, 1859–1877.

Chen, C., H. Liu, and R. C. Beardsley (2003), An unstructured grid, finite-volume, three-dimensional, primitive equations ocean model: Application to coastal ocean and estuaries, *J. Atmos. Oceanic Technol.*, *20*, 159–186.

Chen, C., J. Qi, C. Li, R. C. Beardsley, and H. L. R. W. A. K. Gates (2008), Complexity of the flooding/drying process in an estuarine tidal-creek salt-marsh system: An application of FVCOM, *J. Geophys. Res.*, *113*, C07052, doi:10.1029/2007JC004328.

Ellison, T. H. (1957), Turbulent transport of heat and momentum from an infinite rough plane, *J. Fluid Mech.*, *2*, 456–466.

Garvine, R. W. (1975), The distribution of salinity and temperature in the Connecticut river estuary, *J. Geophys. Res.*, *80*(9), 1176–1183, doi:10.1029/JC080i009p01176.

Geyer, W. R., and D. M. Farmer (1989), Tide-induced variation of the dynamics of a salt wedge estuary, *J. Phys. Oceanogr.*, *19*, 1060–1072.

Geyer, W. R., and J. D. Smith (1987), Shear instability in a highly stratified estuary, *J. Phys. Oceanogr.*, *17*, 1668–1679.

Geyer, W., M. Scully, and D. Ralston (2008), Quantifying vertical mixing in estuaries, *Environ. Fluid Mech.*, *8*, 495–509.

Huang, H., C. Chen, G. W. Cowles, C. D. Winant, R. C. Beardsley, K. S. Hedstrom, and D. B. Haidvogel (2008), FVCOM validation experiments: Comparisons with ROMS for three idealized barotropic test problems, *J. Geophys. Res.*, *113*, C07042, doi:10.1029/2007JC004557.

Ivey, G., and J. Imberger (1991), On the nature of turbulence in a stratified fluid: Part I. The energetics of mixing, *J. Phys. Oceanogr.*, *21*, 650–658.

Jay, D. A., and J. D. Smith (1990a), Residual circulation in shallow estuaries: 1. Highly stratified, narrow estuaries, *J. Geophys. Res.*, *95*(C1), 711–731, doi:10.1029/JC095iC01p00711.

Jay, D. A., and J. D. Smith (1990b), Circulation, density distribution and neap-spring transitions in the Columbia River Estuary, *Prog. Oceanogr.*, *25*, 81–112.

Kantha, L. H., and C. A. Clayson (1994), An improved mixed layer model for geophysical applications, *J. Geophys. Res.*, *99*(C12), 25,235–25,266, doi:10.1029/94JC02257.

Kay, D. J., and D. A. Jay (2003), Interfacial mixing in a highly stratified estuary: 1. Characteristics of mixing, *J. Geophys. Res.*, *108*(C3), 3073, doi:10.1029/2000JC000253.

Li, M., L. Zhong, and W. C. Boicourt (2005), Simulations of Chesapeake Bay estuary: Sensitivity to turbulence mixing parameterizations and comparison with observations, *J. Geophys. Res.*, *110*, C12004, doi:10.1029/2004JC002585.

MacCready, P., and W. R. Geyer (2001), Estuarine salt flux through an isohaline surface, *J. Geophys. Res.*, *106*(C6), 11,629–11,637, doi:10.1029/2001JC900006.

MacCready, P., N. S. Banas, B. M. Hickey, E. P. Dever, and Y. Liu (2009), A model study of tide- and wind-induced mixing in the Columbia River Estuary and plume, *Cont. Shelf Res.*, *29*, 278–291.

MacDonald, D. G., and W. R. Geyer (2004), Turbulent energy production and entrainment at a highly stratified estuarine front, *J. Geophys. Res.*, *109*, C05004, doi:10.1029/2003JC002094. (Available at http://www.agu.org/pubs/crossref/2004/2003JC002094.shtml)

MacDonald, D. G., and A. R. Horner-Devine (2008), Temporal and spatial variability of vertical salt flux in a highly stratified estuary, *J. Geophys. Res.*, *113*, C09022, doi:10.1029/2007JC004620.

MacDonald, D. G., L. Goodman, and R. D. Hetland (2007), Turbulent dissipation in a near-field river plume: A comparison of control volume and microstructure observations with a numerical model, *J. Geophys. Res.*, *112*, C07026, doi:10.1029/2006JC004075.

Mellor, G. L., and T. Yamada (1982), Development of a turbulence closure model for geophysical fluid problems, *Rev. Geophys. Space Phys.*, *20*, 851–875.

Osborn, T. (1980), Estimates of the local rate of vertical diffusion from dissipation measurements, *J. Phys. Oceanogr.*, *10*, 83–89.

Partch, E. N., and J. D. Smith (1978), Time dependent mixing in a salt wedge estuary, *Estuarine Coastal Mar. Sci.*, *6*, 3–19.

Peters, H. (1999), Spatial and temporal variability of turbulent mixing in an estuary, *J. Mar. Res.*, *57*, 805–845.

Peters, H. (2003), Broadly distributed and locally enhanced turbulent mixing in a tidal estuary, *J. Phys. Oceanogr.*, *33*, 1967–1977.

Ralston, D. K., W. R. Geyer, and J. A. Lerczak (2010), Structure, variability, and salt flux in a strongly forced salt wedge estuary, *J. Geophys. Res.*, *115*, C06005, doi:10.1029/2009JC005806.

Rennau, H., and H. Burchard (2009), Quantitative analysis of numerically induced mixing in a coastal model application, *Ocean Dyn.*, *59*, 671–687.

Rodi, W. (1987), Examples of calculation methods for flow and mixing in stratified fluids, *J. Geophys. Res.*, *92*(C5), 5305–5328, doi:10.1029/JC092iC05p05305.

Shih, L. H., J. R. Koseff, G. N. Ivey, and J. H. Ferziger (2005), Parameterization of turbulent fluxes and scales using homogeneous sheared stably stratified turbulence simulations, *J. Fluid Mech.*, *525*, 193–214.

Simpson, J., and D. Bowers (1981), Models of stratification and frontal movement in shelf seas, *Deep Sea Res., Part A.*, *28*, 727–738.

Simpson, J. H., D. J. Crisp, and C. Hearn (1981), The shelf-sea fronts: Implications of their existence and behaviour [and discussion], *Philos. Trans. R. Soc. London, Ser. A*, *302*, 531–546.

Stacey, M. T., S. G. Monismith, and J. R. Burau (1999), Observations of turbulence in a partially stratified estuary, *J. Phys. Oceanogr.*, *29*, 1950–1970.

Trowbridge, J. H., W. R. Geyer, M. M. Bowen, and A. J. Williams (1999), Near-bottom turbulence measurements in a partially mixed estuary: Turbulent energy balance, velocity structure, and along-channel momentum balance, *J. Phys. Oceanogr.*, *29*, 3056–3072.

Umlauf, L., and H. Burchard (2003), A generic length-scale equation for geophysical turbulence models, *J. Mar. Res.*, *61*, 235–265.

Umlauf, L., and H. Burchard (2005), Second-order turbulence closure models for geophysical boundary layers. A review of recent work, *Cont. Shelf Res.*, *25*, 795–827.

Uncles, R. J., and J. A. Stephens (1996), Salt intrusion in the tweed estuary, *Estuarine Coastal Shelf Sci.*, *43*, 271–293.

Wang, B., O. Fringer, S. Giddings, and D. Fong (2009), High-resolution simulations of a macrotidal estuary using SUNTANS, *Ocean Modell.*, *26*, 60–85.

Warner, J. C., W. R. Geyer, and J. A. Lerczak (2005), Numerical modeling of an estuary: A comprehensive skill assessment, *J. Geophys. Res.*, *110*, C05001, doi:10.1029/2004JC002691.

Zhong, L., and M. Li (2006), Tidal energy fluxes and dissipation in the Chesapeake Bay, *Cont. Shelf Res.*, *26*, 752–770.

W. R. Geyer and D. K. Ralston, Applied Ocean Physics and Engineering, Woods Hole Oceanographic Institution, MS 11, Woods Hole, MA 02543, USA. (dralston@whoi.edu)

J. A. Lerczak, College of Oceanic and Atmospheric Sciences, Oregon State University, Corvallis, OR 97331, USA.

M. Scully, Department of Ocean, Earth, and Atmospheric Sciences, Old Dominion University, Norfolk, VA 23529, USA.